Geomechanics and Engineering, *Vol. 43, No. 2 (2025) 99-108*
https://doi.org/10.12989/gae.2025.43.2.099

Failure envelope of square footings resting on cohesive-frictional soils subjected to combined loading

Amirreza Sadeghi and Meysam Imani*

Geotechnical Engineering Group, Amirkabir University of Technology, Garmsar Campus, Iran

(*Received May 8, 2024, Revised October 1, 2025, Accepted October 10, 2025*)

Abstract. The bearing capacity of foundations is one of the most important issues that have always attracted the attention of researchers and geotechnical engineers. In this article, the failure envelope of square footings resting on cohesive-frictional soils was investigated considering the simultaneous application of vertical, horizontal, and moment loads using finite element simulations. The effect of various factors such as soil internal friction angle, cohesion, modulus of elasticity, Poisson's ratio, unit weight and the failure criterion along with the groundwater table, the dimensions and the embedment depth of the footing were investigated. The results show that the soil friction angle has a greater effect on the size of the failure envelope than the soil cohesion. Moreover, the soil modulus of elasticity, Poisson's ratio, unit weight, and the groundwater table, have a minor effect on the size of the failure envelope compared to the footing embedment depth. By moving the footing from the ground surface to a depth equal to three times the footing width, the failure envelope enlarges more than seven times of its initial size.

Keywords: cohesive-frictional soil; combined loading; failure envelope; finite element method; square footing

1. Introduction

Many classical theories have been presented in past studies to determine the bearing capacity of foundations. In such studies, the bearing capacity was obtained considering a single load (vertical, horizontal, or moment). However, the effect of simultaneous application of these loads was considered using a correction factor. More recently, researchers have focused on investigating the effect of simultaneous application of vertical (*V*), horizontal (*H*) and moment (*M*) loads on the bearing capacity of foundations by means of failure envelope approach. The failure envelope represents a two or three-dimensional space considering different combinations of *V*, *H* and *M*. Depending on the applied loads, the failure envelope can be defined in different dimensional spaces like vertical-moment (*VM*), vertical-horizontal (*VH*), and horizontal-moment (*HM*). The three-dimensional space of vertical-horizontal-moment loading (*VHM*) can also be introduced.

The studies performed by Meyerhof (1956), Hansen (1970), Vesic (1975), and Bolton (1979) are among the pioneer researches in the field of bearing capacity under the effect of combined loads. Later, Butterfield and Ticof (1979) conducted several experiments to propose the failure envelope under *HM* loading as an elliptic curve which was used by Dean *et al.* (1992) and Houlsby and Martin (1992) as a basis for estimating the bearing capacity of spudcan foundations under combined loading. Other researchers like Butterfield and Gottardi (1994), Zhang *et al.* (2013), and Sadeghi Fazel and Boluri Bazaz (2020) used experimental methods to consider the effect of different load types, i.e., *V*, *H*, or *M*, on the failure envelope. Analytical methods have also been used to determine the failure envelopes. Among others, one can mention the limit analysis solutions presented by Bransby and Randolph (1997), Houlsby and Puzrin (1999), and Tang and Phoon (2014). The limit equilibrium method has also been used by Afsharpour et al. (2022) to evaluate the ultimate bearing capacity of shallow foundations resting on partially saturated coarse-grained cohesionless and fine-grained cohesive soils. They considered a wide range of combined vertical, horizontal and moment loads.

Because of its abilities, numerical methods play an important role in tackling with the failure envelopes in different loading spaces. Bransby and Randolph (1998) applied the finite element method to develop failure envelopes of cohesive soils subjected to *VH*, *VM*, and *HM* loads. Gourvenec (2007) investigated the effect of different width-to-length ratios of rectangular footings on the bearing capacity under the *VH*, *VM*, and *VHM* loads. Also, Bransby and Yun (2009) investigated the effect of skirted footing dimensions on the undrained bearing capacity subjected to combined loading by performing finite element analysis. Vulpe *et al*. (2013) presented the failure envelope of skirted spudcan foundations under *VHM* using the finite element method. Mehravar *et al*. (2016) evaluated the effect of settlement of caissons on the vertical, horizontal, and moment-bearing capacity using three-dimensional finite element modeling. In addition, different studies are available regarding the failure envelope of circular footings including the Houlsby and Cassidy (2002), Cassidy *et al*. (2002), Shen *et al*. (2016) and Suryasentana *et al.* (2020) methods. Moreover, the behavior of deep foundations subjected to combined loading was also investigated in the literature. Graine *et al*. (2021) applied the finite element

*Corresponding author, Assistant Professor
E-mail: imani@aut.ac.ir

Copyright © 2025 Techno-Press, Ltd.

ISSN: 2005-307X (Print), 2092-6219 (Online)

method to evaluate the bearing capacity of a single pile located in a homogeneous clay under a combination of *VHM* loads. By comparing their numerical results with the available analytical methods, they showed that analytical methods give more conservative results than numerical analysis. Xia *et al.* (2022) used the finite element method to study the bearing capacity of a single pile placed on a layered soil consisting of a soft clay layer underlying by a hard clay layer in *VM* and *VH* loading spaces. Chanda *et al*. (2022) used a numerical approach to investigate the effect of length, diameter, and number of piles on the failure envelope. They have also applied experimental method to consider the failure envelope of a group of piles located on sandy soil. Birid and Choudhury (2022) investigated the behavior of circular and ring foundations placed on cohesive soils under combined loading. By applying Tresca failure criterion for the soil, they considered the effect of the foundation's geometry and changes in the degree of soil heterogeneity on the failure envelopes of the foundations. For two-spaced rectangular foundations with rigid connections, Sun *et al*. (2023) applied three-dimensional finite element analyses to examine the coupled interaction of foundation spacing and degree of soil strength heterogeneity on the load-carrying capacity of the foundation systems under general loading. Cheng *et al*. (2024) employed numerical analyses to investigate the failure mechanisms of hybrid skirted foundations under combined *VHM* loading in silty sand-over-clay deposit. They proposed an empirical approximate expression to estimate the uniaxial and combined bearing capacity of hybrid skirted foundations. Using finite element method, Wang *et al*. (2024) investigated the uniaxial and *VHM* undrained bearing capacity of a new frame-type gravity structure named the gravity tripod foundations.

Reviewing literature shows that most previous researches have focused on cohesive or frictional soils and detailed studies on the failure envelope of cohesive-frictional soils have rarely been conducted. Therefore, in this paper, the failure envelope for a square footing resting on cohesive-frictional soil was obtained using three-dimensional finite element modeling. The effect of various parameters like soil geotechnical parameters, the footing dimensions and embedment depth, and the groundwater table on the failure envelope were investigated.

2. Numerical modeling

2.1 Model specification

Fig. 1 shows the general configuration of the finite element model constructed in this research by the Plaxis 3D code. The model comprises 27259 ten-noded elements. An elastic square footing with the width B was considered on the top of the model, which is under the effect of vertical (V), horizontal (H), and moment (M) loads. The dimensions of the meshes and the distance of the model boundaries from the footing edges were determined by trial and error so that the magnitudes beyond them do not have a considerable effect on the results. The hardening soil model was used for the soil.

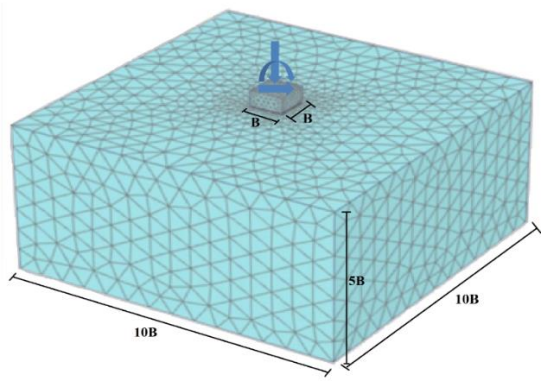

Fig. 1 General configuration of the finite element model

2.2 Drawing the failure envelope

For drawing the failure envelope in *VH*, *VM*, and *HM* spaces, different ratios of v/h, $v/B\theta$ and $h/B\theta$ should be applied to the footing, respectively. The values of v, h and θ are the ultimate magnitudes of vertical, horizontal, and moment loads, respectively, which can be tolerated by the soil under the footing. For drawing the failure envelope, the vertical load-settlement, horizontal load-horizontal displacement, and moment-rotation curves should be drawn for the center point under the footing. Then, using the tangent intersection method proposed by Trautmann and Kulhawy (1988), the values of v, h and θ can be derived from the curves. Afterward, the ratios v/h, $v/B\theta$ and $h/B\theta$ should be set equal to nB, where n has any arbitrary value. As a result, the remaining unknown parameters can be determined. For example, to draw the *VM* failure envelope, by assuming $n=\pm 0.5B$, θ can be obtained as follows

$$\frac{v}{B\theta} = \pm 0.5B \rightarrow \theta = \frac{v}{0.5B^2} \tag{1}$$

By considering different values of n, a set of points with the coordinates (v, θ) can be obtained in the two-dimensional space *VM*, in which the failure envelope can be drawn by connecting them.

3. Comparison of the results with other solutions

To enhance the reliability of the findings presented in this study, extensive comparative analyses were conducted between the current results and those reported by previous researchers. These comparisons encompass a range of soil types, including cohesive, frictional, and cohesive–frictional soils. Furthermore, the analyses include load–settlement and moment–rotation curves, as well as failure envelopes, all of which are discussed in subsequent sections.

3.1 Comparison with load-settlement and moment-rotation curves

Al-Dawoodi *et al*. (2021) applied a finite element model to obtain the load-settlement curve of a square footing resting on a cohesive-frictional soil with a width equal to 80

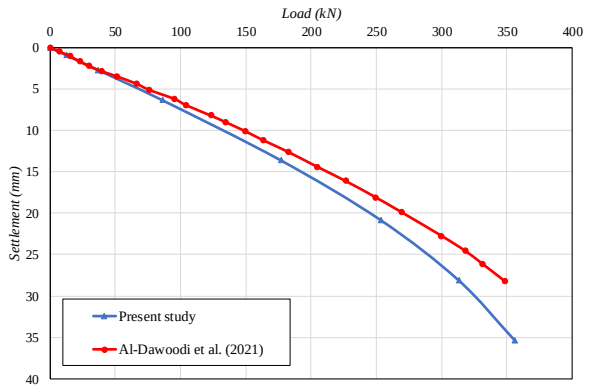

Fig. 2 Comparison of the vertical load-settlement curve of the present paper with Al-Dawoodi *et al.* (2021) method

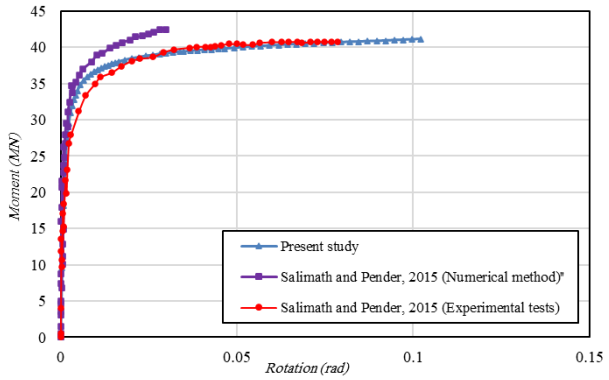

Fig. 3 Comparison of bending moment-rotation curves obtained from different methods

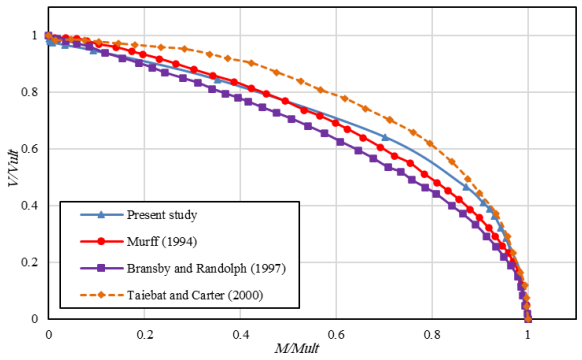

Fig. 4 Comparison of V/V_{ult}-M/M_{ult} envelope obtained from different methods

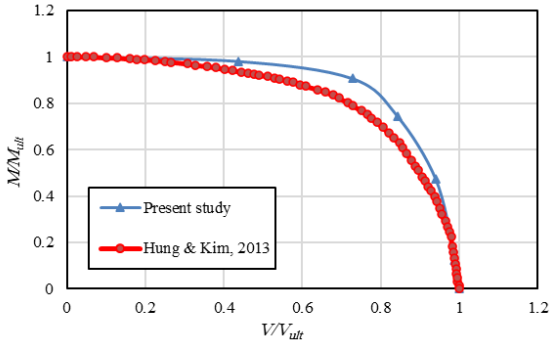

Fig. 5 Comparison of the results of current research with the method of Hung and Kim (2013)

cm located on a soil with a unit weight equal to 15 kN/m^3, the modulus of elasticity of 10000 kN/m^2, the Poisson's ratio of 0.4, and the cohesion and internal friction angle equal to 70 kN/m^2 and 10°, respectively. Considering the same assumptions, a finite element model was constructed in the present paper, and the results were compared in Fig. 2. The results derived from both approaches exhibit a consistent trend, with the maximum deviation between them reaching approximately 20%.

Using finite element analysis, Salimath and Pender (2015a) investigated the behavior of a rectangular footing located on clay under the simultaneous effect of a constant vertical load and an increasing bending moment. Also, Salimath and Pender (2015b) built a laboratory model to investigate the same issue experimentally. The same model was constructed numerically in the current study, and the results are compared in Fig. 3. As can be seen, there is a good agreement among the results, especially between the results of the present paper and the experimental method used by Salimath and Pender (2015b).

3.2 Comparison of the failure envelopes

Using the finite element method, Taiebat and Carter (2000) calculated the *VM* failure envelope of a circular footing located on a cohesive soil. Same studies were performed by Murff (1994) and Bransby and Randolph (1997). In these studies, the soil unit weight was considered equal to 16 kN/m^3, and the undrained cohesion of s_u = 5 kPa, the modulus of elasticity of $E = 300s_u$ = 1500 kN/m^2, and the Poisson's ratio of 0.49 were considered. Fig. 4 shows the comparison of the results. V_{ult} and M_{ult} are the ultimate vertical load and bending moment that the footing can tolerate, respectively. As can be seen, the failure envelope obtained from the present paper stands among the curves obtained by other researchers and all of them have a similar variation trend.

Hung and Kim (2013) applied the finite element method to obtain the V/V_{ult} -M/M_{ult} envelope of a bucket footing resting on a clay with a unit weight of 16 kN/m^3. The soil modulus of elasticity was considered equal to 6.25 kN/m^2 at the ground surface which increased in depth. The undrained cohesion of 70 kN/m^2, and the Poisson's ratio of 0.495 were also considered. Fig. 5 compares the present study and the Hung and Kim (2013) method. The maximum differences between the M/M_{ult} and V/V_{ult} ratios of the two methods are 23% and 7%, respectively.

Another comparison was performed with the Larsen (2008) experimental and numerical studies that deal with the moment-rotation behavior of bucket footings on sand. He considered a sand with a unit weight of 20 kN/m^3, modulus of elasticity of 15000 kN/m^2, cohesion of 1 kN/m^2, internal friction angle of 47.5°, dilation angle of 2°, and the Poisson's ratio of 0.3. Using the same properties in the present study, Fig. 6 compares the results. The curve obtained from the present study is in close agreement with

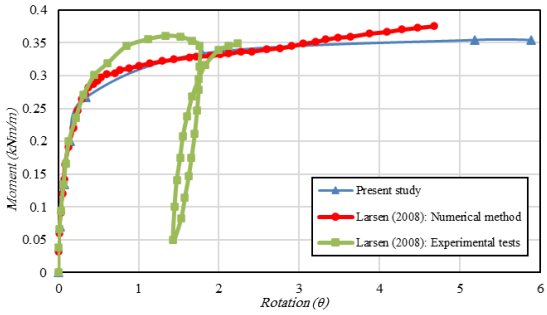

Fig. 6 Comparison of the results of present paper with the Larsen (2008) methods

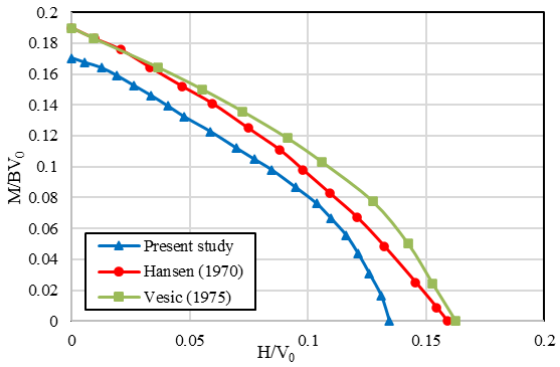

Fig. 7 Comparison of present study with the classical methods of bearing capacity

Table 1 Parameters used for comparison

Footing	Diameter, B (m)	5
	Embedment depth, D (m)	0
Soil	Modulus od Elasticity, E (MPa)	40
	Friction angle, ϕ (°)	30
	Cohesion, c (kPa)	50
	Unit weight, γ (kN/m^3)	18

the curve obtained from the numerical method of Larsen (2008), while all three methods show approximately similar results at the initial part of the moment-rotation curve. It should be noted that in the experimental method used by Larsen (2008), the unloading-reloading of the bending moment was considered, while in his numerical method and also in the present paper only the loading procedure was applied.

3.3 Comparison with classical methods of determining the bearing capacity

The classical methods of determining the bearing capacity, such as the famous methods proposed by Hansen (1970) and Vesic (1975), provide the possibility of determining the bearing capacity under the effect of combined loads. For a circular foundation located on a soil with the specifications according to Table 1, Fig. 7 shows a comparison among the results. The size of the failure envelope resulting from the present study is smaller than those obtained from the classical methods, which indicates that the classical methods result in more conservative bearing capacity magnitudes.

Table 2 Initial parameters used for parametric analyses

Parameters	Soil type A	Soil type B	Soil type C
E (MPa)	70	40	10
c' (kPa)	100	50	25
ϕ' (°)	40	30	20
ψ (°)	10	0	0

4. Parametric analyses

In this section, the effects of various parameters on the failure envelope resulting from the simultaneous application of V, H, and M were investigated. As mentioned in Table 2, three soil types were considered. Soil type A represents more strength than others, while the weakest soil is type C. The parameter ψ represents the soil dilation angle. The analyses were performed for a square footing with a width equal to two meters resting on top of the soil bedding.

4.1 Effect of the soil cohesion

For the soil type B, the effect of soil cohesion on the *HM* envelope was investigated. It was assumed that V/V_{ult} = 0.5. The first step for drawing the failure envelope is drawing the curves shown in Fig. 8. Using the tangent intersection method proposed by Trautmann and Kulhawy (1988), the ultimate values of the vertical, horizontal, and moment loads as well as their corresponding displacements and rotations were calculated, which are presented in Table 3.

Using the procedure described in Section 2.2, the *HM* failure envelope was plotted in Fig. 9(a). Also, the dimensionless envelope with respect to the ultimate values of H_{ult} and M_{ult} was shown in Fig. 9(b). By increasing the soil cohesion from 25 kPa to 100 kPa, the size of the *HM* failure envelope became three times larger. In the dimensionless H/H_{ult}-M/M_{ult} envelope, the maximum enlargement is about 7%, which occurred in the second and fourth regions of the coordinate system. In these regions, the horizontal displacement of the footing has an opposite direction with the rotation caused by the moment. Therefore, the soil has more bearing capacity to withstand the applied load. However, in the regions one and three, the same direction of the horizontal displacement and the rotation caused the underlying soil weaker in a way that variation of the cohesion does not have considerable effect on the size of the failure envelope.

Using the same procedure as described in this section, the effect of various parameters on the failure envelopes were investigated in the following sections.

4.2 Effect of the soil internal friction angle

For the soil type B and considering V/V_{ult} = 0.5, the

Table 3 ultimate values of vertical, horizontal, and moment loads and their corresponding displacements and rotation

Cohesion (kPa)	Vertical loading		Horizontal loading		Bending Moment loading	
	Ultimate Load, V_{ult} (kN)	Corresponding Displacement, v (mm)	Ultimate Load, H_{ult} (kN)	Corresponding Displacement, h (mm)	Ultimate Bending Moment, M_{ult} (kN.m)	Corresponding Rotation, θ (deg)
25	2200	42	180	3	200	0.2
50	3500	65	265	4	350	0.3
100	6300	125	400	6	620	0.4

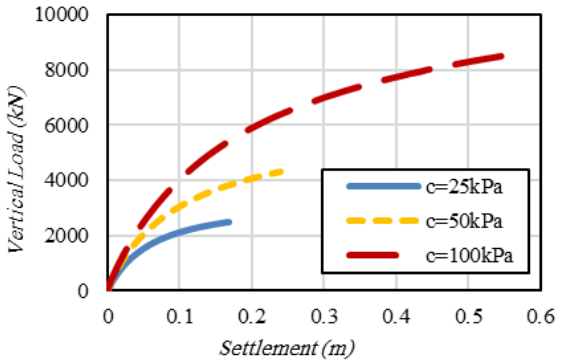

(a) Vertical load – Settlement curve

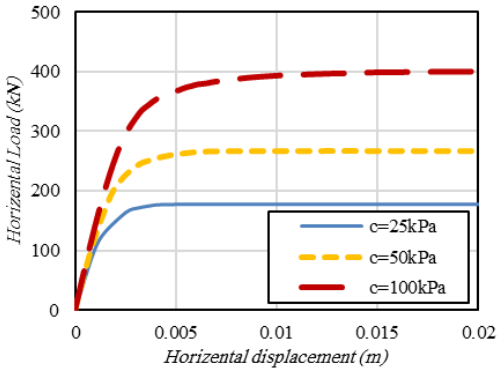

(b) Horizontal load – Horizontal displacement curve

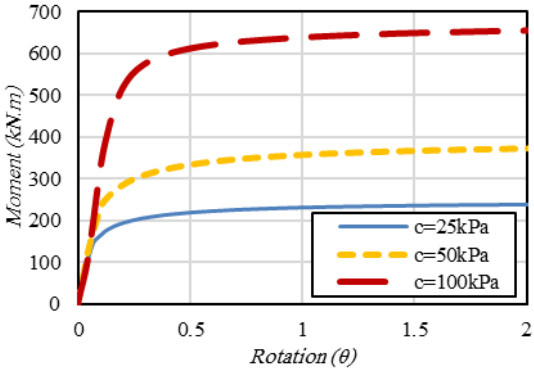

(c) Bending moment – Rotation curve

Fig. 8 Effect of soil cohesion on the response of square footing subjected to different values of load and moment

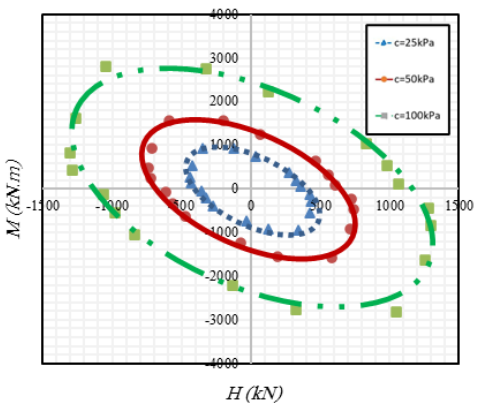

(a) *HM* failure envelope

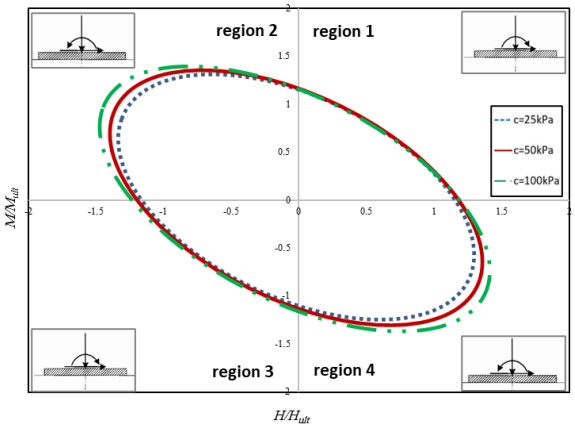

(b) H/H_{ult}-M/M_{ult} failure envelope

Fig. 9 Effect of the soil cohesion on failure envelopes

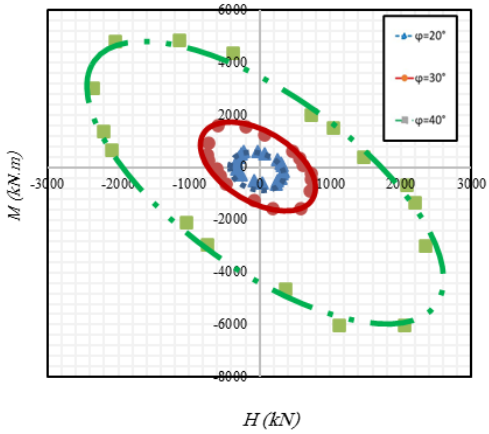

(a) *HM* failure envelope

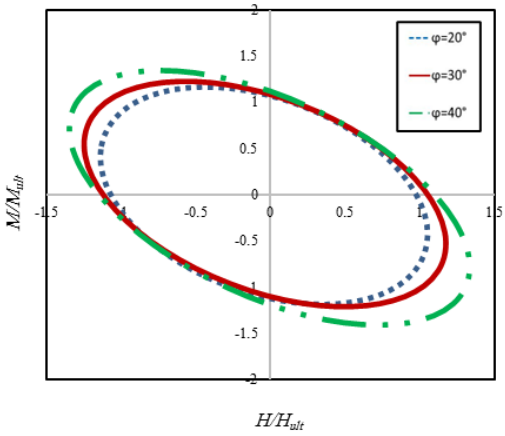

(b) H/H_{ult}-M/M_{ult} failure envelope

Fig. 10 Effect of the soil internal friction angle on failure envelopes

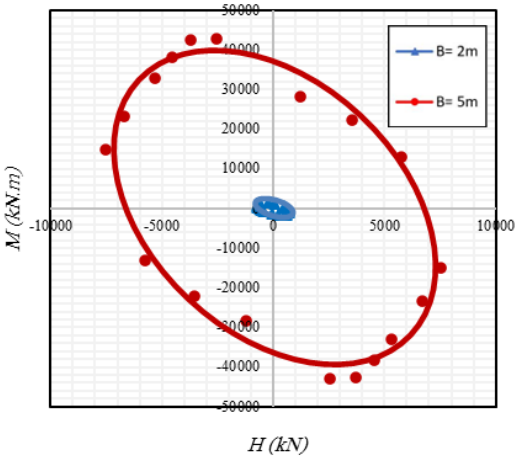

(a) *HM* failure envelope

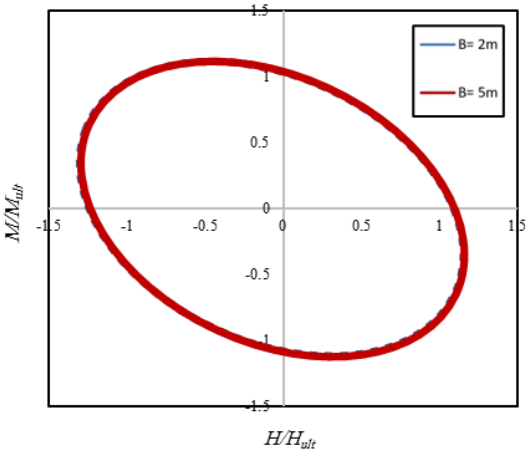

(b) H/H_{ult}-M/M_{ult} failure envelope

Fig. 11 Effect of the footing width on failure envelopes

effect of soil internal friction angle was investigated, considering ϕ° equals to 20°, 30° and 40°. As the soil internal friction angle increases from 20° to 40°, the interlocking between soil particles becomes stronger, results in enhancing the soil's load-bearing capacity. Therefore, the *HM* failure envelope became about six times larger (Fig. 10(a)), while the maximum enlargement of the dimensionless envelope was about 22% (Fig. 10(b)), which occurred in the second and fourth regions of the coordinate system. The reason for the difference between the size variation of the dimensionless envelope in the second and forth regions compared to the first and third regions is similar to what was explained in the previous section.

4.3 Effect of the footing width

The effect of the footing width on the failure envelope was investigated by considering two different magnitudes for the footing width. For the soil type B and assuming V/V_{ult} = 0.5, by increasing the footing width from 2 to 5 meters, the *HM* failure envelope became eight times larger (Fig. 11(a)), while the size of the normalized failure envelope became unchanged (Fig. 11(b)), which shows that the footing width has an equal effect on both the H-H_{ult} and M-M_{ult} magnitudes.

4.4 Groundwater effect

In order to investigate the effect of groundwater on the failure envelope, both dry and saturated conditions were considered for the soil type B in the case of V/V_{ult} = 0.5. According to Fig. 12(a), the *HM* failure envelope of the dry soil is about 8% to 12% larger than that of saturated soil in different regions of the coordinate system. Fig. 12(b) shows that the dimensionless envelope of the dry case is about 7% larger than that of the saturated soil in the regions two and four of the coordinate system.

4.5 Effect of the soil modulus of elasticity

To investigate the effect of soil modulus of elasticity on the failure envelope, the magnitudes equal to 10, 40, and 70 MPa were considered for the soil type B assuming V/V_{ult} =

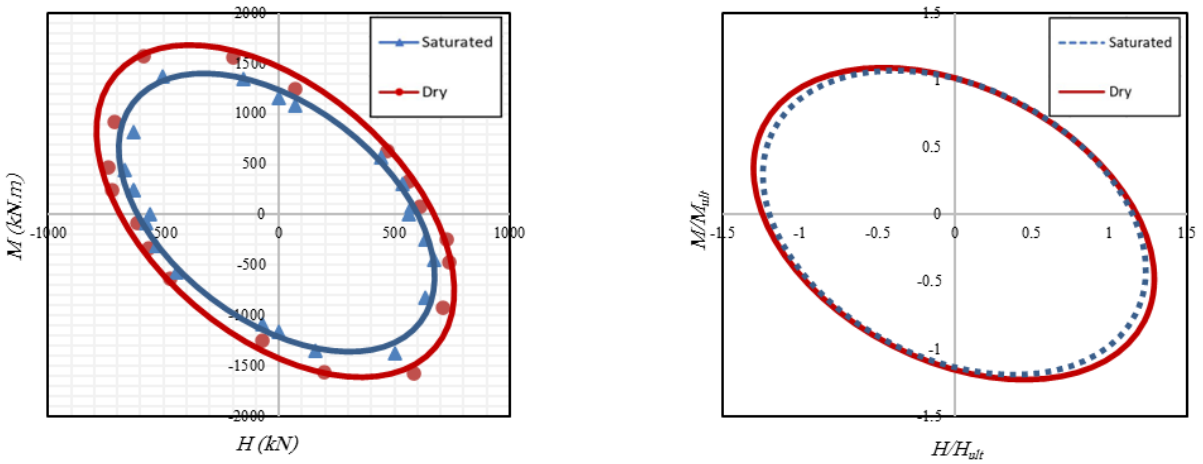

(a) *HM* failure envelope (b) H/H_{ult}-M/M_{ult} failure envelope

Fig. 12 Effect of the groundwater on failure envelopes

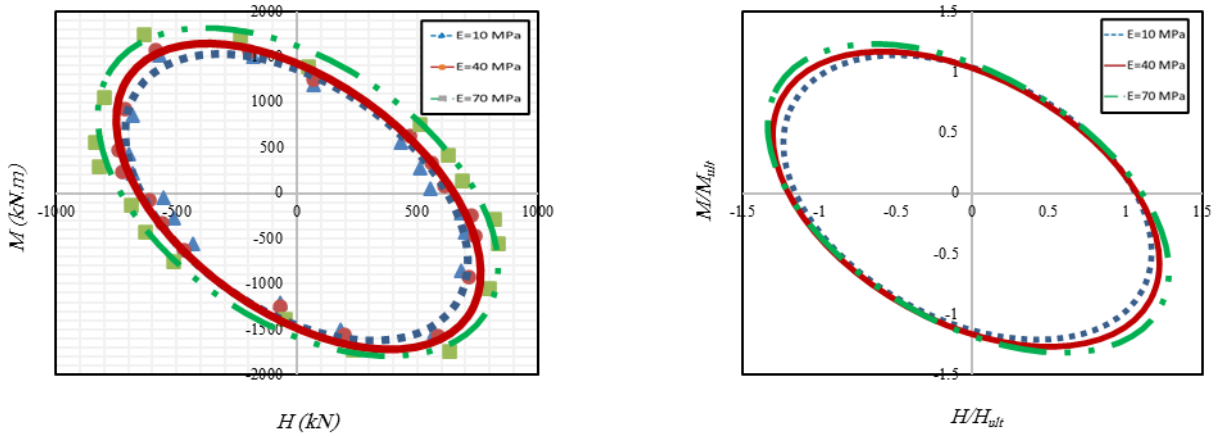

(a) *HM* failure envelope (b) H/H_{ult}-M/M_{ult} failure envelope

Fig. 13 Effect of soil modulus of elasticity on failure envelopes

0.5. For the model that was used in the current practice, the unloading-reloading modulus was considered to be three times the elasticity modulus. According to Fig. 13(a), with increasing the modulus of elasticity, the size of the *HM* failure envelope increased by a maximum of 18%, while the dimensionless envelope enlarged by about 12% in the regions two and four of the coordinate system.

4.6 Effect of the soil failure criterion

The analyses performed in the current study are based upon the Hardening Soil model. However, the effect of the failure criterion was investigated by considering the Mohr-Coulomb failure model. Considering the soil type B and assuming $V/V_{ult} = 0.5$, Fig. 14 compares the envelope for the two failure criteria. As shown in Fig. 14(a), the envelope obtained from the Mohr-Coulomb failure criterion is about 33% larger than that obtained from the Hardening Soil criterion, which shows the bigger load-carrying capacity derived from the Mohr-Coulomb criterion. A reverse result can be seen from the dimensionless envelopes in Fig. 14(b), in which the envelope obtained from the Mohr-Coulomb model is about 12% smaller than that of the Hardening Soil model. This conclusion shows that the Mohr-Coulomb failure criterion overestimates the ultimate values of H and M (i.e., H_{ult} and M_{ult}), which results in smaller H/H_{ult} and M/M_{ult} ratios than those obtained from the Hardening Soil model.

4.7 Effect of the footing embedment depth

The effect of the footing embedment depth (D_f) was also investigated. For the soil type B and assuming $V/V_{ult} = 0.5$, Fig. 15 shows the results. By increasing the embedment depth from zero to 1.5 times the footing width, the *HM* failure envelope enlarges approximately three times, while an embedment equal to three times the footing width results in an envelope approximately seven times that of the case of the footing resting on the ground surface. It is interesting to note that increasing the embedment depth results in anticlockwise rotation of the failure envelope. This conclusion means that by increasing the embedment depth

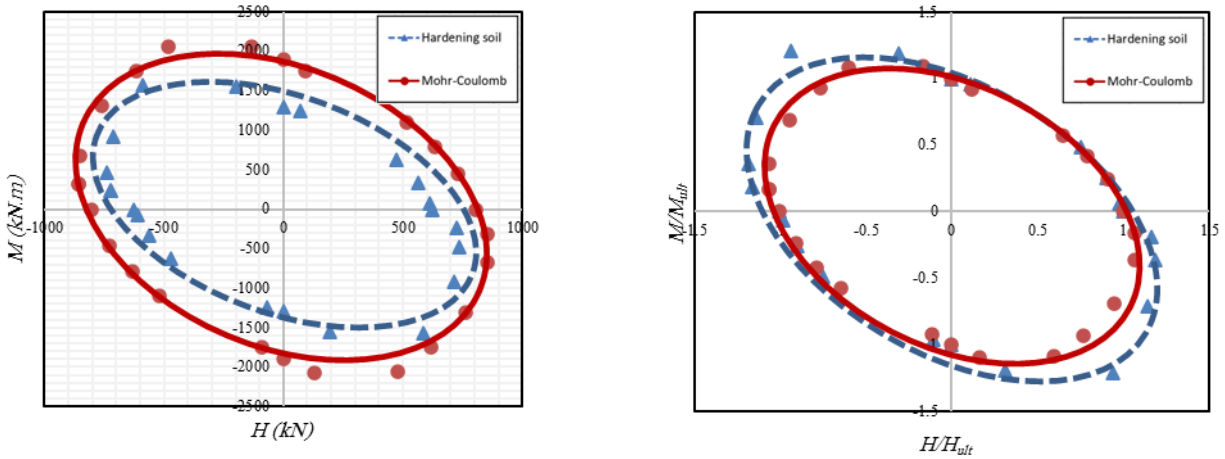

(a) *HM* failure envelope (b) H/H_{ult}-M/M_{ult} failure envelope

Fig. 14 Effect of the soil failure criterion on failure envelopes

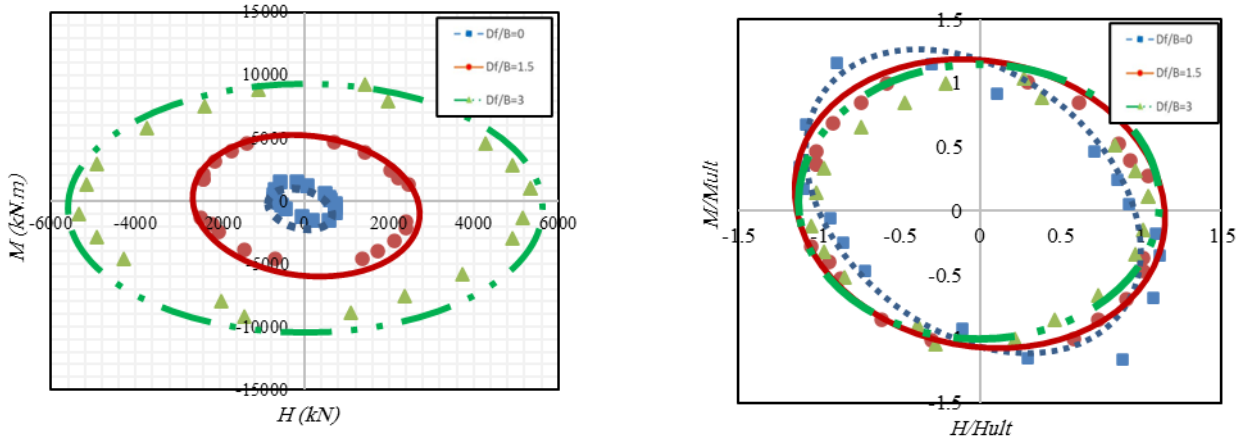

(a) *HM* failure envelope (b) H/H_{ult}-M/M_{ult} failure envelope

Fig. 15 Effect of the footing embedment depth on failure envelopes

of the footing (D_f), the sameness of the direction of the horizontal displacement (due to H) and the rotation (due to M) does not affect the failure envelope considerably, which in turn, results in symmetry of the envelope with respect to the horizontal and vertical axes and turning its shape from an oval to a circle.

4.8 Effect of V/V_{ult} on the HM failure envelope

In order to investigate the effect of vertical load ratio (V/V_{ult}) on the *HM* failure envelope, different values of this ratio, including zero, 0.25, 0.5, 0.75, and 0.9, were considered. For the soil type B, Fig. 16 shows the *HM* failure envelopes for dry and saturated cases. For both cases, by increasing V/V_{ult} from zero to 0.5, the *HM* failure envelope expands, while for V/V_{ult} from 0.5 to 0.9 it becomes smaller, reaching the vertical axis as a single point. This finding shows that by increasing the vertical load ratio up to V/V_{ult} = 0.5, the ability of the footing to withstand the combination of horizontal and moment loads increases. However, with further increase in this ratio (i.e., further increase of V), most soil resistance mobilizes to tolerate the vertical load. In contrast, minor resistance remains for H and M, which results in the reduction of the *HM* envelope.

5. Conclusions

The main conclusions of the present study include:

- Among the considered soil parameters (c, ϕ, and E), the internal friction angle (ϕ) has the greatest effect on the H/H_{ult}-M/M_{ult} failure envelope. By increasing ϕ from 20° to 40°, the size of the dimensionless failure envelope increases by 22%. Among the soil properties, the least effect is related to the soil cohesion (c), which by increasing it from 25 kPa to 100kPa, the H/H_{ult}-M/M_{ult} failure envelope enlarges by 7%.
- Among the considered geometrical parameters of the problem, the greatest effect on H/H_{ult}-M/M_{ult} failure envelope is related to the groundwater level. The size of the dimensionless failure

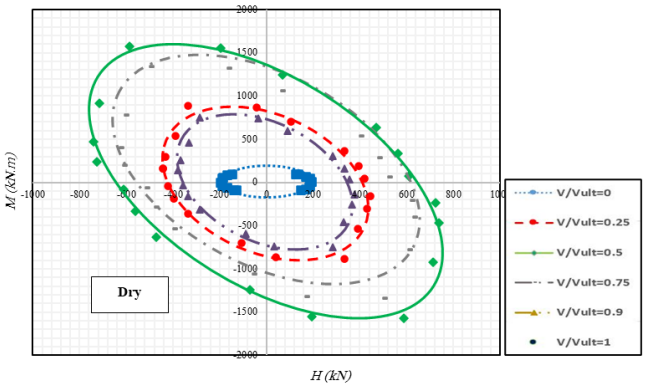

(a) Dry soil

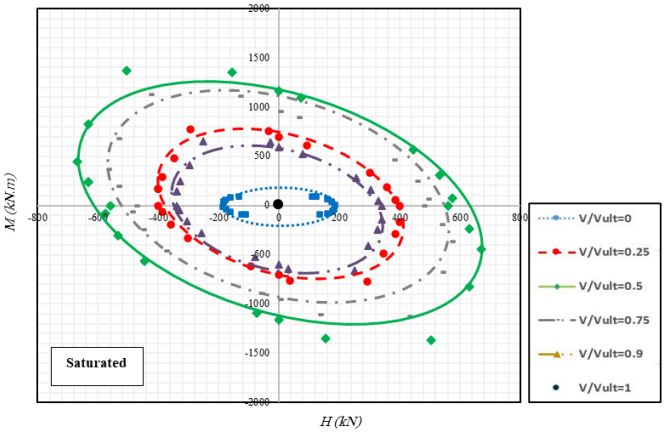

(b) Saturated soil

Fig. 16 Effect of V/V_{ult} on HM failure envelope of soil

envelope in the dry state is 7% larger than that of the saturated state. Also, the least effect is related to the footing width. By increasing B, the size of the dimensionless failure envelope remains constant.

- The results show that the size of the failure envelope resulting from the Mohr-Coulomb failure criterion is larger than that of the hardening soil failure criterion. However, in the case of dimensionless failure envelope, a reverse conclusion was obtained.
- The results show that by increasing the vertical load ratio V/V_{ult} from zero to 0.5, the size of the failure envelope becomes larger. Beyond the magnitude of V/V_{ult}=0.5, the failure envelope becomes smaller by increasing V, which indicates that at high values of the vertical load, the failure envelope is less affected by V and is more dependent on H and M magnitudes.
- An increase in vertical load does not necessarily enhance the horizontal bearing capacity of the foundation. In other words, increasing the weight of the structure does not guarantee that the foundation will be able to resist greater horizontal loads and moments.
- The failure envelopes presented in this study, which incorporate various subsoil characteristics, offer a valuable design and evaluation framework for square footings under combined V-H-M loading. These results provide engineers with a more nuanced understanding of foundation behavior under realistic loading scenarios.

References

Afsharpour, S., Payan, M., Jamshidi Chenari, R., Ahmadi, H. and Fathipour, H. (2022), "Bearing capacity of strip footings on unsaturated soils under combined loading using LEM", *Geomech. Eng.*, **31**(2), 223-235. https://doi.org/10.12989/gae.2022.31.2.223.

Al-Dawoodi, A.B., Rahil, F.H. and Waheed, M.Q. (2021), "Numerical simulation of shallow foundation behavior rested on sandy soil", *IOP Conference Series: Earth and Environmental Science*, **856**(1), 210-240. https://doi.org/10.1088/1755-1315/856/1/012042.

Birid, K. and Choudhury, F.D. (2022), "Failure envelopes for ring foundations resting on tresca soil under combined loading", *Geotech. Geoenviron. Eng.*, **148**(11), https://doi.org/10.1061/(ASCE)GT.1943-5606.0002900.

Bolton, M.D. (1979), "A guide to soil mechanics", Macmillan, London.

Bransby, M.F. and Randolph, M.F. (1997), "Shallow foundations subject to combined loadings", *Proceedings of the 9th Int. Conf. Comput. Methods Adv. Geomech*, Wuhan, China.

Bransby, M.F. and Randolph, M.F. (1998), "Combined loading of skirted foundations", *Géotechnique*, **48**(5), 637-655. https://doi.org/10.1680/geot.1998.48.5.637.

Bransby, M.F. and Yun, G.J. (2009), "The undrained capacity of

skirted strip foundations under combined loading", *Ge'otechnique*, **59**(2), 115-125. https://doi.org/10.1680/geot.2007.00098.

Butterfield, R. and Gottardi, G. (1994), "A complete three-dimensional failure envelope for shallow footing on sand", *Geotechnique*, **44**(1), 181-184. https://doi.org/10.1680/geot.1994.44.1.181.

Butterfield, R. and Ticof, J. (1979), "Design parameters for granular soils (discussion contribution)", *Proceedings of the 7th European Conf. on Soil Mech. and Foundation Eng.*, Brighton, U.K.

Chanda, D., Saha, R., Haldar, S., Nayak, C.B. and Kumar, V. (2022), "Scaled modeled tests and finite element numerical study on lateral responses of PRF system under V-H-M loading", *Geomech. Geoeng.*, **18**(4), 1-25. https://doi.org/10.1080/17486025.2022.2048092.

Cheng, H., Niu, F., Zhou, M., Zhang, X., Tian, Y. and Li, J. (2024), "Bearing capacity of hybrid skirted foundations in silty sand-over-clay under combined VHM loading", *Int. J. Geomech.*, **24**(8), 04024154. https://doi.org/10.1061/IJGNAI.GMENG-9283.

Dean, E.H., James, R.G., Schofield, A.S., Tan, F.S.C. and Tsukamoto, Y. (1992), "The bearing capacity of conical footing on sand in relation to the behaviour of spudcan footings of jack-ups", *Proceedings of the Wroth Memorial Symp. "Predictive Soil Mechanics"*, Oxford, U.K., Thomas Telford, London, U.K.

Gourvenec, S. (2007), "Shape effects on the capacity of rectangular footings under general loading", *Géotechnique*, **57**(8), 637-646. https://doi.org/10.1680/geot.2007.57.8.637.

Graine, N., Hjiaj, M. and Krabbenhoft, K. (2021), "3D failure envelope of a rigid pile embedded in a cohesive soil using finite element limit analysis", *Int. J. Numer. Anal. Method. Geomech.*, **45**(2), 265-290. https://doi.org/10.1002/nag.3152.

Hansen, B. (1970), "A revised and extended formula for bearing capacity", *Bulletin of Danish Geotechnical Institute*, Copenhagen 28, 5-11.

Houlsby, G.T. and Cassidy, M.J. (2002), "A plasticity model for the behaviour of footings on sand under combined loading", *Géotechnique*, **52**(2), 117-129. https://doi.org/10.1680/geot.2002.52.2.117.

Houlsby, G.T. and Martin, C.M. (1992), "Modeling of the behaviour of foundations of jack-up units on clay", *Proceedings of the Wroth Memorial Symp. "Predictive Soil Mechanics"*, Oxford, U.K.

Houlsby, G.T. and Purzin, A.M. (1999), "The bearing capacity of strip footing on clay under combined loading", *Proc. Roy. Soc.* **455**(1983), 893-916. https://doi.org/10.1098/rspa.1999.0340.

Hung, L.C. and Kim, S.R. (2013), "Evaluation of undrained bearing capacities of bucket foundations under combined loads", *Mar. Georesour. Geotec.*, **32**(1), 76-92. https://doi.org/10.1080/1064119X.2012.735346.

Larsen, K.A. (2008), "Static behaviour of bucket foundations", PhD Thesis, Aalborg University, Denmark.

Mehravar, M., Harireche, O. and Faramarzi, A. (2016), "Evaluation of undrained failure envelopes of caisson foundations under combined loading", *Appl. Ocean Res.*, **59**, 129-137. https://doi.org/10.1016/j.apor.2016.05.001.

Meyerhof, G.G. (1953), "The bearing capacity of foundations under eccentric and inclined loads", *Proceedings of the 3rd International Conference on Soil Mechanics and Foundation Engineering*.

Murff, J.D. (1994), "Limit analysis of multi-footing foundation systems". *Proceedings of the computer methods and advanced geomechanics*, Morgantown, Rotterdam.

Sadeghi Fazel, A.H. and Bolouri Bazaz, J. (2020), "An experimental investigation of ring footings resting on granular material subject to combined V-H-M loading", *Amirkabir J. Civil Eng.*, **53**(4), 1607-1622. doi:10.22060/CEEJ.2020.17071.6450.

Salimath, R.S. and Pender, M.J. (2015a), "Moment-rotation behavior of shallow foundations with fixed vertical load using PLAXIS 3D", *Proceedings of the 6th International Conference on Earthquake Geotechnical Engineering*, New Zealand.

Salimath, R.S. and Pender, M.J. (2015b), "Plaxis modelling of moment-rotation curves for shallow foundations on clay at constant vertical load", *Proceedings of the 12th Conference on Geomechanics*, New Zealand.

Sun, L., Sun, Q., Feng, X., Tang, C. and Lang, R. (2023), "Undrained capacity of two rigidly connected rectangular foundations under general V-H-M loading", *Comput. Geotech.*, **161**, 105613. https://doi.org/10.1016/j.compgeo.2023.105613.

Suryasentana, S.K., Dunne, H.P., Martin, C.M., Burd, H.J., Byrne, B.W. and Shonberg, A. (2020), "Assessment of numerical procedures for determining shallow foundation failure envelopes", *Géotechnique*, **70**(1), 60-70. https://doi.org/10.1680/jgeot.18.P.055.

Taiebat, H.A. and Carter, J.P. (2000), "Numerical studies of the bearing capacity of shallow foundations on cohesive soil subjected to combined loading", *Géotechnique*, **50**(4), 409-418. https://doi.org/10.1680/geot.2000.50.4.409.

Tang, C., Phoon, K.K. and Toh, K.C. (2014), "Effect of footing width on Nγ and failure envelope of eccentrically and obliquely loaded strip footings on sand", *Can. Geotech. J.*, **52**(6), 694-707. https://doi.org/10.1139/cgj-2013-0378.

Vesic, A.S. (1975), "Bearing capacity of shallow foundations", *Foundation Engineering Handbook 1st Ed.*, (Eds., H.F. Winterkorn and H.Y. Fang), Chapter 3, Van Nostrand Reinhold Company, Inc., New York, N.Y.

Vulpe, C., Bienen B. and Gaudin C. (2013), "Predicting the undrained capacity of skirted spudcans under combined loading", *Ocean Eng.*, **74**, 178-188. https://doi.org/10.1016/j.oceaneng.2013.06.027.

Wang, J., Yan, Y., Fu, D. and Zhou, Z. (2024), "Bearing capacity of the gravity tripod foundation under general loading in clay", *Ocean Eng.*, **295**, 116883. https://doi.org/10.1016/j.oceaneng.2024.116883.

Xia, H., Zhou, M., Niu, F., Zhang, X. and Tian, Y. (2022), "Combined bearing capacity of bucket foundations in soft-over-stiff clay", *Appl. Ocean Res.*, https://doi.org/10.1016/j.apor.2022.103299.

Zhang, Y., Bienen, B and Cassidy, M.J. (2013), "Development of a combined VHM loading apparatus for a geotechnical drum centrifuge", *Int. J. Phys. Model. Geotech.*, **13**(1), 13-30. https://doi.org/10.1680/ijpmg.12.00007.

GC